

Article

Wavelengths of the Self-Photopumped Nickel-Like $4f\ ^1P_1 \rightarrow 4d\ ^1P_1$ X-ray Laser Transitions

Elena Ivanova

Institute of spectroscopy of RAS, Physicheskaya st., 5, Troitsk, 108840 Moscow, Russia; eivanova@isan.troitsk.ru

Academic Editor: Joseph Reader

Received: 31 January 2017; Accepted: 27 June 2017; Published: 13 July 2017

Abstract: The energies for the lower $3d_{3/2}4d_{3/2}$ [$J = 1$] and upper $3d_{3/2}4f_{5/2}$ [$J = 1$] working levels in the self-photopumped X-ray laser are analyzed along the Ni-like sequence. We have found some irregularities in these energy levels in the range $Z = 42\text{--}49$. The causes of the irregularities are studied. The list of elements that lase on the self-photopumped transition can be extended much further than originally known. We calculate the wavelengths of this transition in Ni-like sequence to $Z = 79$ using the relativistic perturbation theory with a zero approximation model potential. We estimate the wavelength accuracy for $Z > 50$ as $\Delta\lambda/\lambda \leq 0.005$.

Keywords: X-ray lasers; spectroscopy of multicharged ions; self-photo pumped lasers

1. Introduction

Self-photo pumped (SPP) X-ray lasers (XRL) in Ni-like ions were presented in 1996 [1] as an alternative approach to the standard radiative collisional scheme for inversion creation. We use the term SPP following the name given in literature. This is really a collisionally pumped laser assisted by radiation trapping. Both schemes for Ni-like ions are shown in Figure 1. This new class of SPP in Ni-like XRL was first investigated theoretically in [2], where high gain was predicted for the $4f\ ^1P_1\text{--}4d\ ^1P_1$ transition in Mo^{14+} at 22.0 nm. It was supposed that preplasma was created by a nanosecond pulse followed by a picosecond pulse to control the temperature and density in plasma, and to achieve high gain. This wavelength was calculated using the multiconfiguration Dirac-Fock atomic physics code by Grant and co-workers in the extended average level mode [3]. In the experiment [4], the Ni-like SPP XRL on the $4f\ ^1P_1\text{--}4d\ ^1P_1$ transition was demonstrated in Zr, Nb, and Mo, and the measured wavelengths for these ions were presented. For Mo^{14+} a gain of 13 cm^{-1} was measured at 22.6 nm for a target up to 1 cm long [4]. The wavelengths of this transition for ions from $Z = 36$ to 54 were predicted in [4] using the experimental data of this work to provide small corrections to their calculations. In the experiment [5], the progress in the optimization and understanding of the collisional pumping of X-ray lasers using an ultrashort subpicosecond heating pulse was reported. Time-integrated and time-resolved lasing signals at the standard $4d\ ^1S_0\text{--}4p\ ^1P_1$ XRL line in Ni-like Ag were studied in detail. Under specific irradiation conditions, strong lasing was obtained on the SPP $4f\ ^1P_1\text{--}4d\ ^1P_1$ transition at 16.1 nm. The strong lasing on the SPP transition in Mo^{14+} was also observed with very modest (less than 1 J) pump energy at a high repetition rate [6]. Recently, lasing on the SPP $3d\ ^1P_1\text{--}3p\ ^1P_1$ laser line has been observed for Ne-like V, Cr, Fe, and Co, as well as for Ni-like Ru, Pd, and Ag [7]. A strong dependence on the delay between the main and second prepulse was found: the optimum delay shifts towards smaller delays with increasing atomic number Z . Accurate wavelength measurements and calculations were shown to be in excellent agreement. The experiment [7] demonstrated that the list of elements that lase on the SPP transitions can be extended much further than originally known.

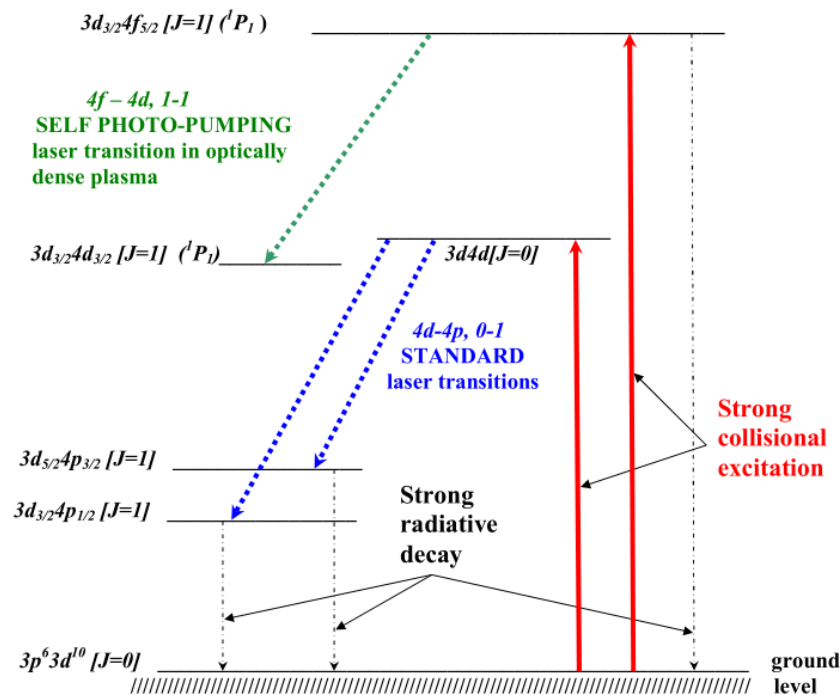


Figure 1. Schematic diagram of three low XRL transitions in Ni-like ions.

Many authors have investigated the spectra of Ni-like ions using vacuum sparks, laser produced plasma and electron beam ion traps as light sources [8–14]. The $3d^9 4d$ and $3d^9 4f$ configurations have been analyzed in the Rb X–Mo XV sequence [10,11]. In [10,11], these configurations were investigated using parameter extrapolations within the Generalized-Least-Squares (GLS) method. This method was used in [12,13] to predict for $3d^9 4d$, $3d^9 4f$ configuration energy levels in Cd XXI and Ag XX. GLS predictions of $3d^9 4d$, $3d^9 4f$ energy levels in the Zr XIII–Pd XIX sequence are tabulated in [14].

Note that lasing wavelength (λ_{las}) in Mo^{14+} was determined theoretically [2] and in the experiment [4] using one and the same atomic physics code [3], but results for λ_{las} were somewhat different (by 4 Å). The $3d_{3/2} 4f_{5/2} [J = 1]$ upper working level has the largest oscillator strength and radiative transition probability to the $3d^{10}$ ground level. This fact allows it to achieve high precision in this level energy measurement along the Ni-like sequence up to high $Z \sim 84$; in some ions, the energy of the transition to the ground state was accurate up to the fourth significant digit. The wavelengths of resonant radiative transitions in heavy Ni-like ions were calculated by us to $Z = 83$ in [15]. Moreover, in [15], the wavelengths (for Z within 79–82) were predicted with the same accuracy, although they have not yet been measured experimentally.

In the present paper, we analyze the smoothness of the working energy levels of SPP XRL along the Ni-like sequence. We found some irregularities in Ni-like sequence energies in the region $Z = 42$ (Mo^{14+}) and in the region $Z = 49$ (In^{21+}) for the upper $3d_{3/2} 4f_{5/2} [J = 1]$ working level. The causes of the irregularities are studied.

The principle purpose of this paper is to predict the wavelengths of SPP XRL lines in Ni-like ions with $Z \leq 79$. The calculations are performed by the Relativistic Perturbation Theory with Model Zero Approximation, (RPTMP). The fundamental principles of the RPTMP approach are given in [16]. Energy levels of the $3p^6 3d^9 4l$, $3p^5 3d^{10} 4l$, ($l = 0, 1$) configurations and radiative transition rates to the $3p^6 3d^{10}$ ground state in the Kr IX ion are calculated by this method in [16]. The stability of calculations on the approximation used is shown in [16].

2. Features of Lower and Upper Working Levels of SPP XRL along the Ni-Like Sequence

The schematic diagram of three strong XRL transitions is shown in Figure 1: two of them are standard $3d4d [J = 0] - 3d_{5/2}4p_{3/2} [J = 1]$ and $3d4d [J = 0] - 3d_{3/2}4p_{1/2} [J = 1]$ transitions. The classifications of lower working levels in Figure 1 are valid for $Z > 42$. The $3d_{5/2}4p_{3/2} [J = 1]$ level is the lower working level of an XRL for the entire nickel isoelectronic sequence, the $3d_{3/2}4p_{1/2} [J = 1]$ level is the lower working level for heavy ions starting with $Z = 62$. The third $3d_{3/2}4p_{3/2} [J = 1]$ level decays to a ground state significantly weaker than the two mentioned above, and does not provide a significant gain. In our recent work [17], the energies of standard XRL transitions in ions of the Ni-like sequence with $Z \leq 79$ are refined by RPTMP calculations. The calculated energies of the two standard $4d-4p$, $J = 0-1$ XRL transitions are corrected by extrapolation of the experimental differentials of XRL transition energies $dE_Z^{las} = E_Z^{las} - E_{Z-1}^{las}$, i.e., the differences between transition energies of neighboring ions, which weakly depend on Z (especially in the region $Z \leq 50$). It is proven that the accuracy for the final results for large Z is within the experimental error.

The $3d_{3/2}4f_{5/2} [J = 1] - 3d_{3/2}4d_{3/2} [J = 1]$ transition is optically self-photopumped XRL in all Ni-like ions, the positions of working levels vary with respect to other levels along the sequence. Based on our previous studies of XRL [18–20], it can be argued that there are at least four principal differences between standard and self photo-pumped mechanisms:

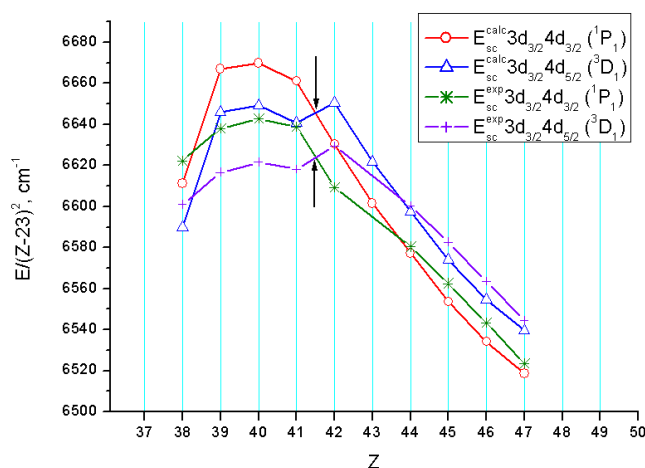
- (1) In the standard scheme, the upper working level is populated by strong monopole electron collisions: in the SPP scheme it is populated by strong dipole electron collisions, which means high oscillator strength and effective photoabsorption.
- (2) Effective SPP XRL is possible only in optically thick plasma (large electron density n_e and diameter d), while the standard XRL is possible both in optically thick and in optically thin plasma over a wide range of n_e and d .
- (3) In the SPP, the upper working level is quickly emptied due to the large radiative decay rate. Therefore, in this scheme, a laser effect is short-lived; maximum XRL duration may be a few tens of picoseconds. A standard XRL can operate in quasi-continuous mode (under certain conditions).
- (4) In the SPP, the lower and upper working levels do not change their classification along the Ni-like sequence; in the standard scheme the upper working level changes its classification: the $3d_{5/2}4d_{5/2} [J = 0]$ state is dominant in the classification of the upper working level at $Z \leq 51$, and the $3d_{3/2}4d_{3/2} [J = 0]$ state is dominant for $Z > 51$ [17].

Below, we demonstrate the irregularities in the sequence of both the lower and the upper working levels of SPP XRL. Crossing of each working level with another level causes these irregularities. Level crossing is accompanied by a strong interaction at certain Z points. Figure 2a shows the scaled energies along Z of the $3d_{3/2}4d_{3/2} [J = 1]$ lower working level and the $3d_{3/2}4d_{5/2} [J = 1]$ level close to it. In addition to the energy levels calculated here, Figure 2a also shows the corresponding experimental values [14]. Reference [14] does not indicate classification of $3d4d [J = 1]$ levels, their classification was made earlier in [11]. Note that theoretical and experimental classifications are identical. There are some differences between theoretical and experimental energies, typically a few units in the 4th–5th digits. These differences are conditioned by the shift of the theoretical list of energy levels as a whole, but this shift does not affect the accuracy of λ_{las} . The energy levels in Figure 2a are scaled by dividing by $(Z-23)^2$, so that the behavior of the third and fourth significant digits can be observed. At the beginning of the sequence, the $3d_{3/2}4d_{3/2} [J = 1]$ level is above the $3d_{3/2}4d_{5/2} [J = 1]$ level. The crossing of these levels is in the range $41 < Z < 42$ (shown by arrows). The crossing of the corresponding experimental energy levels occurs at exactly the same Z values. At $Z = 42$, one can observe the “repulsion” of levels caused by their interaction; the “repulsion” is a feature of theoretical and experimental data. Note, that repulsion can be seen due to energy scaling; in fact, the repulsion value is approximately a few thousand cm^{-1} , i.e., a few units in the fourth digit for the $3d_{3/2}4d_{5/2} [J = 1]$ level.

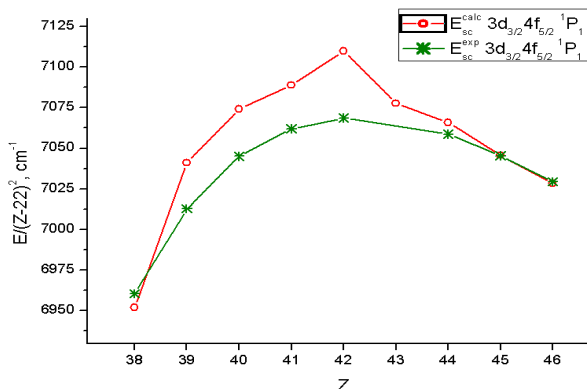
In Figure 2b, we can see hard-to-explain behavior of the $3d_{3/2}4f_{5/2} [J = 1]$ upper working level in the region of $Z = 42$. The features of this level will be considered below in more detail; however,

it is important to note, here, that the energy structure of odd states in the range $Z = 40\text{--}49$ exhibits extremely high instability caused by the interaction of levels with each other, which rapidly changes with Z . In the case at hand, we understand the instability as the ambiguity of the calculation of eigenvectors and eigenenergies. As a result, the calculation in the same approximation leads to different energies at a certain level. The deviation from the smooth curve in Figure 2a is $\sim 10,000\text{ cm}^{-1}$; however, such a value leads to a sufficiently large deviation from the corresponding experimental values of λ_{las} shown in Figure 3.

At the point $Z = 42$, λ_{las} calculated here is $\sim 222\text{ \AA}$, which is smaller than the experimental and theoretical values of [4] by 4 \AA . In a recent experiment [7], the delay time between preliminary and main pump pulses was optimized to achieve the maximum yield of the X-ray laser. In fact, the electron density was optimized in [7]. X-ray lasing occurs in the Ni-like ion ionization mode, so that the lasing times on both transitions were restricted to the ionization time of Ni-like ions to the Co-like state. Time-resolved measurements in [7] allowed high-accuracy wavelength measurements of the SPP and standard X-ray laser lines. Thus, the calculations of the previous work [4] were confirmed: $\lambda_{las} \approx 22.61\text{ nm}$ in Ni-like molybdenum (Mo^{14+} , $Z = 42$). Our calculations are performed for an isolated atom. Based on the studies performed, it can be argued that the interaction of levels at the point $Z = 42$ is so strong that the energy levels $3d_{3/2}4d_{3/2} [J = 1]$, $3d_{3/2}4d_{5/2} [J = 1]$ in dense hot plasma can differ significantly from the corresponding energy levels in an isolated atom.



(a)



(b)

Figure 2. (a) Theoretical and experimental crossing of low working $3d_{3/2}4d_{3/2} [J = 1]$ energy level with $3d_{3/2}4d_{5/2} [J = 1]$ energy level in Ni-like sequence, shown by scaled energy values along Z .; (b) Features of theoretical upper working level $3d_{3/2}4f_{5/2} [J = 1]$, shown by scaled energy along Z in comparison with correspondent experimental data.

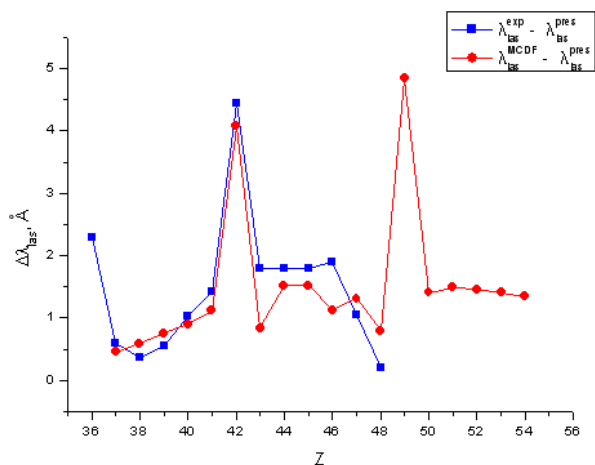


Figure 3. Difference between experimental, predicted from [4] and calculated here, λ_{las} of SPP XRL transitions in Ni-like ions.

The problem is the composition of the $3d_{3/2}4d_{3/2} [J = 1]$ working level, which indicates the strength of level interaction. It is shown in Figure 4 for all $3d4d [J = 1]$ levels in Ni-like ions with $Z = 36-79$. Figure 4 shows that contributions of the $3d_{3/2}4d_{3/2} [J = 1]$ and $3d_{3/2}4d_{5/2} [J = 1]$ levels are almost equal at $Z = 42$, which could lead to levels' misidentification. Theoretical energies of these levels at $Z = 42$ are $2,393,554 \text{ cm}^{-1}$ and $2,400,846 \text{ cm}^{-1}$ (51% and 41%, respectively, are the contributions to the $3d_{3/2}4d_{3/2} [J = 1]$ low working level). The contributions of these levels in [11] are 45% and 34%, and the energies are $2,385,902 \text{ cm}^{-1}$ and $2,393,229 \text{ cm}^{-1}$ respectively. (We note that the theoretical list of energies of Ni-like ions in the range of small Z is shifted as a whole by $5000-8000 \text{ cm}^{-1}$). Figure 4 demonstrates the rapid restructuring of lower working level compositions: so that the $3d_{5/2}4d_{3/2} [J = 1]$ level contribution increases by five orders of magnitude in the range $Z = 40-42$.

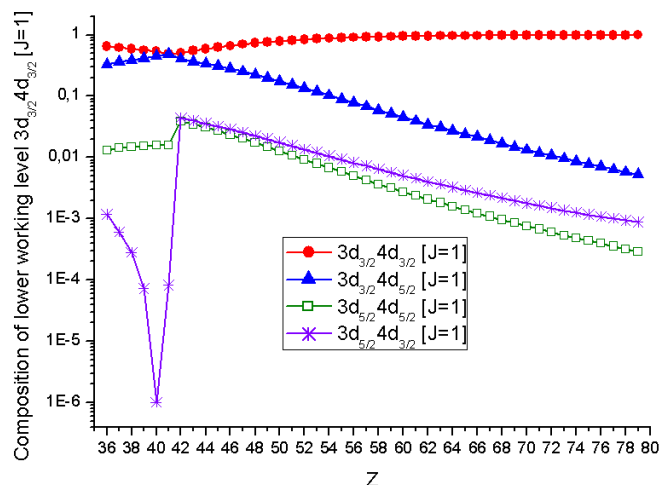


Figure 4. Composition of lower working level $3d_{3/2}4d_{3/2} [J = 1]$ along Ni-like sequence on a logarithmic scale.

Figure 5 shows the scaled energies along Z of the $3d_{3/2}4f_{5/2} [J = 1]$ upper working level and the close $3p_{3/2}4s_{1/2} [J = 1]$ level. Crossing of these levels occurs in the range $48 < Z < 49$. At $Z = 49$ one can see the “repulsion” of levels caused by their interaction; the “repulsion” is a feature of theoretical data. In Figure 5, the corresponding experimental energies for the $3d_{3/2}4f_{5/2} [J = 1]$ level are shown [14]. Unfortunately, we have no available data on the experimental $3p_{3/2}4s_{1/2} [J = 1]$ levels in the Z region under consideration. The value $Z = 49$ is the point of an abrupt jump (irregularity) in spectroscopic

constants of the $3d_{3/2}4f_{5/2} [J = 1]$ upper working level and the $3p_{3/2}4s_{1/2} [J = 1]$ level crossing it, caused by the strong interaction of these levels at this value of Z . This interaction is shown in Figure 6, where we can see the $3d_{3/2}4f_{5/2} [J = 1]$ level composition. The interaction of levels at the point $Z = 49$ leads to the so-called effect of oscillator strength transfer we considered in [21] for the Ne-like sequence. At this point, the rate of radiative processes abruptly changes: the probabilities of the transition from the $3d_{3/2}4f_{5/2} [J = 1]$ level to the ground state and to the state of the lower working level slightly decrease. At the same time, these probabilities for the $3p_{3/2}4s_{1/2} [J = 1]$ level increase by an order of magnitude and become almost equal in magnitude to the corresponding values of the $3d_{3/2}4f_{5/2} [J = 1]$ level. It can be assumed that there was an incorrect identification at the point $Z = 49$ when extrapolating the upper working level in [4], and the $3p_{3/2}4s_{1/2} [J = 1]$ level that is close to the $3d_{3/2}4f_{5/2} [J = 1]$ level in energy was used as the upper working level (see Figure 5). If this assumption is correct, $\lambda_{las} \sim 144.7 \text{ \AA}$ for $Z = 49$, which is identical to [4]. When using our value for $3d_{3/2}4f_{5/2} [J = 1]$, $\lambda_{las} \sim 140.0 \text{ \AA}$ (here the energy jump shown in Figure 5 is taken into account). Another argument in favor of the incorrect identification in [4], are large jumps of the differential $d\lambda_{las}(Z) = \lambda_{las}(Z) - \lambda_{las}(Z-1)$ in the range $Z = 47-50$.

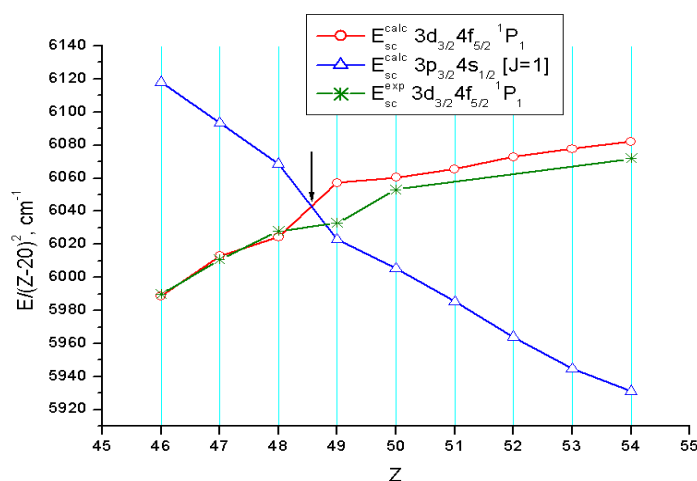


Figure 5. Crossing of upper working $3d_{3/2}4f_{5/2} [J = 1]$ energy level with $3p_{3/2}4s_{1/2} [J = 1]$ energy level in Ni-like sequence, shown by scaled energy values along Z . The corresponding experimental values for $3d_{3/2}4f_{5/2} [J = 1]$ energies are also shown.

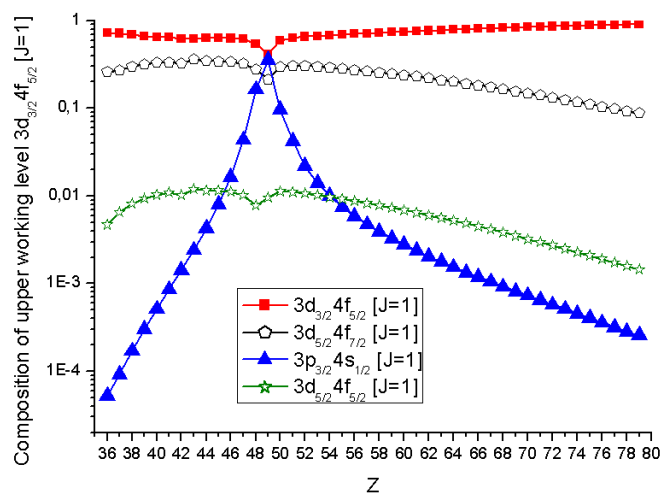


Figure 6. Composition of upper working level $3d_{3/2}4f_{5/2} [J = 1]$ along Ni-like sequence on a logarithmic scale.

3. Wavelengths of the Self-Photopumped Nickel-Like $4f^1P_1 \rightarrow 4d^1P_1$ X-ray Laser Transitions

A comparison of the wavelengths of the self-photopumped nickel-like $4f^1P_1 \rightarrow 4d^1P_1$ X-ray laser transitions, calculated using the RPTMP method with corresponding experimental values and shown in Figure 3, exhibits a deviation of $\leq 1\%$ in the range $Z = 37\text{--}46$. For $Z \geq 48$ Å, our results are identical to experimental data, with an accuracy of several units in the fourth significant digit. Two values of Z are exceptions: (i) the calculation instability point at $Z = 42$; and (ii) the point $Z = 49$, where the $3d_{3/2}4f_{5/2} [J = 1]$ and $3p_{3/2}4s_{1/2} [J = 1]$ states are probably incorrectly identified in the calculation by the MCDF method in [4]. We estimated the accuracy of the calculation of the energies of the upper and lower working states for high Z using experimental measurements of various studies. As an example, we compared the experimental energies for $Z = 74$ (W^{46+}), obtained using the Super EBIT (electron beam ion trap) [22,23], presented in Table 1. There are also listed the theoretical results calculated using the MCDF method called Grasp92 [24]. Here, we do not present earlier calculations of other authors. We also note the impossible comparison to the other calculations [25] in view of the level identification entanglement in this paper.

Table 1. Energy levels (10^3 cm^{-1}) of W XLVII. Comparison of present calculations with experimental data [22,23] and with calculations by GRASP92 [24].

Configuration	Term	J	Experiment	Present Work	GRASP92
$3p^63d^{10}$	1S_0	0	0.0	0.0	0.0
$3p^63d^94s$	$(5/2,1/2)$	3	12,601.5	12,600.1	
		2	12,616.44	12,615.2	12,591.1
$3p^63d^94s$	$(3/2,1/2)$	1	13,138.66	13,137.8	13,110.8
		2	13,148.2	13,147.4	13,120.7
$3p^63d^94p$	$(5/2,1/2)$	2	13,379.05	13,357.5	
		3	13,388.20	13,366.3	
$3p^63d^94p$	$(3/2,1/2)$	2	13,916.27	13,894.8	
		1	13,940.6	13,922.4	13,930.6
$3p^63d^94p$	$(5/2,3/2)$	1	14,229.0	14,234.9	14,221.0
$3p^63d^94p$	$(3/2,3/2)$	1	14,751.0	14,756.2	14,741.1
$3p^63d^94d$	$(3/2,3/2)$	1		15,935.9	15,924.2
$3p^63d^94d$	$(5/2,5/2)$	1	15,556.1	15,561.3	15,550.2
		2	15,610.2	15,614.9	15,605.0
$3p^53d^{10}4s$	$(3/2,1/2)$	1	16,247.0	16,258.9	
$3p^63d^94d$	$(3/2,3/2)$	0	16,256.2	16,284.7	16,282.9
$3p^63d^94f$	$(5/2,7/2)$	1	17,045.9	17,042.2	17,030.6
			17,574.7		
$3p^63d^94f$	$(3/2,5/2)$	1	17,580.3 *	17,586.5	17,585.6
$3p^53d^{10}4s$	$(1/2,1/2)$	1	18,727	18,726.4	18,724.4
$3p^53d^{10}4d$	$(3/2,3/2)$	1	19,044.4	19,041.8	19,057.5
$3p^53d^{10}4d$	$(3/2,5/2)$	1	19,244.5	19,234.8	19,244.1
$3p^53d^{10}4f$	$(3/2,7/2)$	2	20,589.0	20,600.1	20,613.8
$3p^53d^{10}4d$	$(1/2,3/2)$	1	21,561.0	21,547.0	21,614.6

* Data from [23].

Good agreement between experimental and theoretical results for the energy levels in Table 1 may be noted: the maximum deviation is two units in the fourth significant digit. For the problem under study, it is important to ascertain the high accuracy of the calculation of the upper and lower working levels. For the experimental energy of the $3d_{3/2}4f_{5/2} [J = 1]$ level, Table 1 gives two values: one obtained in the experiments [22], and the other later [23]. The difference with our calculation is 6 units in the fifth significant digit. We did not find the experimental energy of the $3d_{3/2}4d_{3/2} [J = 1]$ lower working level for high Z in the literature. The energies of two other states of the $3d4d$ configuration with $J = 1, 2$, given in Table 1, also agree with high accuracy, which indirectly confirms the calculation

reliability. Wavelengths of the $3d_{3/2}4f_{5/2} (^1P_1)-3d_{3/2}4d_{3/2} (^1P_1)$ SPP laser transitions in Ni-like sequence calculated by RPTMP are listed in Table 2.

Table 2. Wavelengths (λ_{las} , Å) of the $3d_{3/2}4f_{5/2} (^1P_1)-3d_{3/2}4d_{3/2} (^1P_1)$ SPP laser transitions in Ni-like sequence calculated by RPTMP.

Z	λ_{las}
50	134.08
51	128.12
52	122.54
53	117.39
54	112.66
55	108.36
56	104.295
57	100.51
58	96.98
59	93.68
60	90.57
61	87.65
62	84.89
63	82.28
64	79.81
65	77.47
66	75.23
67	73.08
68	71.06
69	69.11
70	67.25
71	65.47
72	63.75
73	62.10
74	60.51
75	58.97
76	57.48
77	56.04
78	54.64
79	53.23

4. Conclusions

The data on λ_{las} (see Table 2) were obtained a priori, no fittings were used. The error could be several units in the fourth significant digit. The precision wavelengths of laser transitions are necessary, in particular, to determine ions in which intense laser emission is possible at wavelengths for which multilayer mirrors (MM) with high reflectance are developed. At least three values of λ_{las} are of interest from the viewpoint of the development of XRL-based sources for nanolithography.

- (i) For $Z = 50$, $\lambda_{las} \sim 134.1$ Å. For this wavelength region, MMs for nanolithography were developed as early as in 1993 [26]. The maximum normal incidence reflectivity achieved that time was 66% for a Mo/Si MM at $\lambda = 13.4$ nm, the reflectivity can be increased to 70%.
- (ii) For $Z = 54$ $\lambda_{las} \sim 11.3$ nm. A series of normal-incidence reflectance measurements at just longer than the beryllium K-edge (11.1 nm) from Mo/Be MM was reported in [27]. The highest peak reflectance was $68.7 \pm 0.2\%$ at $\lambda = 11.3$ nm obtained from a MM with 70 bilayers ending in beryllium. Our model of the high efficient monochromatic radiation sources near $\lambda = 13.5$ at 11.3 nm obtained in Xe^{26+} , intended for commercial nanolithography, was presented in our recent work [28].
- (iii) In Ni-like Ytterbium ($Z = 70$), $\lambda_{las} \approx 67.25$ Å. MM for wavelengths of 6.71–6.89 nm were developed in [29]. Summary of measured and calculated reflectivity of La/B MM for these wavelengths is listed in Table 1 of [29]. The largest reflectivity was observed and calculated for $\lambda = 6.71$ –6.74 nm.

The crossing region of each working level with another level is characterized by their strong effect on each other, which can cause strong instability of the energy structure in the crossing region. In such regions, jumps in functions of energy levels and probabilities of radiative transition on Z are possible (see Figure 2a). The authors of [30], where the level crossing in the Ni-like sequence and associated irregularities in the functions of energies and probabilities of radiative transitions in the range $Z = 74\text{--}84$ were studied, arrived at the same conclusion. From this, the conclusion regarding the possible incorrect identification of levels in their crossing regions follows.

The SPP XRL can be very sensitive to external fields. It is implied that even an insignificant change in the plasma density can affect the emission spectrum. The remarkable phenomenon (see Figure 4) where a rapid increase in the contribution of the $3d_{5/2}4d_{3/2} [J = 1]$ level to the composition of the lower working level is demonstrated could be an indirect confirmation of this. In the interval $Z = 40\text{--}42$, the contribution of this level increases by five orders of magnitude. A similar pattern is observed in Figure 6, where the contribution of $3p_{3/2}4s_{1/2} [J = 1]$ also rapidly increases to $Z = 49$, where this level strongly interacts with the upper working level. In this case, the oscillator strength is transferred from the upper working level to the $3p_{3/2}4s_{1/2} [J = 1]$ level.

Conflicts of Interest: The authors declare no conflict of interest.

References

1. Nilsen, J. Self photo-pumped neon-like and nickel-like X-ray lasers. In Proceedings of the Fifth International Conference on X-Ray Lasers, Lund, Sweden, 10–14 June 1996; Svanberg, S., Walström, C.-G., Eds.; CRC Press: Boca Raton, FL, USA, 1996.
2. Nilsen, J. Design of a picosecond laser-driven Ni-like Mo X-ray laser near 20 nm. *J. Opt. Soc. Am. B* **1997**, *14*, 1511–1514. [[CrossRef](#)]
3. Grant, I.P.; McKenzie, B.J.; Norrington, P.H.; Mayers, D.F.; Pyper, M.C. An atomic multiconfigurational Dirack-Fock package. *Comput. Phys. Commun.* **1980**, *21*, 207–231. [[CrossRef](#)]
4. Nilsen, J.; Dunn, J.; Osterheld, A.L.; Li, Y. Lasing on the self-photopumped nickel-like $4f^1P_1\text{--}4d^1P_1$ X-ray transition. *Phys. Rev. A* **1999**, *60*, R2677–R2680. [[CrossRef](#)]
5. Kuba, J.; Klisnick, A.; Ros, D.; Fourcade, P.; Jamelot, G.; Miquel, J.-L.; Blanchot, N.; Wyart, J.-F. Two-color transient pumping in Ni-like silver at 13.9 and 16.1 nm. *Phys. Rev. A* **2000**, *62*, 043808. [[CrossRef](#)]
6. Luther, B.M.; Wang, Y.; Larotonda, M.A.; Alessi, D.; Berrill, M.; Marconi, M.C.; Rocca, J.J.; Shlyaptsev, V.N. Saturated high-repetition rate 18.9 nm table top laser in Ni-like molybdenum. *Opt. Lett.* **2005**, *30*, 165–167. [[CrossRef](#)] [[PubMed](#)]
7. Siegrist, M.; Staub, F.; Jia, F.; Feuer, T.; Balmer, J.; Nilsen, J. Self-photopumped X-ray lasers from elements in the Ne-like and Ni-like ionization state. *Opt. Commun.* **2017**, *382*, 288–293. [[CrossRef](#)]
8. Reader, J.; Aquista, N.; Kaufman, V. Spectrum and energy levels of seven-times-ionized krypton (Kr VIII) and resonance lines of eight-times-ionized krypton. *J. Opt. Soc. Am. B* **1991**, *8*, 538–547. [[CrossRef](#)]
9. Chen, H.; Beiersdorfer, P.; Fournier, K.B.; Träbert, E. Soft X-ray spectra of highly charged Kr ions in an electron-beam ion trap. *Phys. Rev. E* **2002**, *65*, 056401. [[CrossRef](#)] [[PubMed](#)]
10. Churilov, S.S.; Ryabtsev, A.N.; Wyart, J.-F. Identification of $n = 4$, $\Delta n = 0$ transitions in the spectra of Nickel-like and Zn-like ions through tin. *Phys. Scr.* **1988**, *38*, 326–335. [[CrossRef](#)]
11. Ryabtsev, A.N.; Churilov, S.S.; Nilsen, J.; Li, Y.; Dunn, J.; Osterheld, A.L. Additional analysis of Ni-like ions spectra. *Opt. Spectrosc.* **1999**, *87*, 197–202. (In Russian)
12. Rahman, A.; Hammarsten, E.C.; Sakadzic, S.; Rocca, J.J.; Wyart, J.-F. Identification of $n = 4$, $\Delta n = 0$ transitions in the spectra of Nickel-like cadmium ions from a capillary discharge plasma column. *Phys. Scr.* **2003**, *67*, 414–419. [[CrossRef](#)]
13. Rahman, A.; Rocca, J.J.; Wyart, J.-F. Classification of the Nickel-like silver spectrum (Ag XX) from a fast capillary discharge plasma. *Phys. Scr.* **2004**, *70*, 21–25. [[CrossRef](#)]
14. Churilov, S.S.; Ryabtsev, A.N.; Wyart, J.-F. Analysis of the 4–4 transition in the Ni-like Kr IX. *Phys. Scr.* **2005**, *71*, 457–463. [[CrossRef](#)]
15. Ivanova, E.P.; Gogava, A.L. Energies of X-ray transitions in heavy Ni-like ions. *Opt. Spectrosc.* **1985**, *59*, 1310–1314. (In Russian)

16. Ivanova, E.P. Energy levels and probability of radiative transitions in the Kr IX ion. *Opt. Spectrosc.* **2014**, *117*, 179–187. [[CrossRef](#)]
17. Ivanova, E.P. Wavelengths of the $4d-4p$, $0-1$ X-ray laser transitions in Ni-Like ions. *Int. J. Adv. Res. Phys. Sci.* **2016**, *3*, 34–40. [[CrossRef](#)]
18. Ivanova, E.P. Proposal for precision wavelength measurement of the Ni-like gadolinium X-ray laser formed during the interaction of nanostructured target with an ultrashort laser beam. *Laser Phys. Lett.* **2015**, *12*, 105801. [[CrossRef](#)]
19. Ivanova, E.P.; Zinoviev, N.A.; Knight, L.V. Theoretical investigation of X-ray laser on the transitions of Ni-like xenon in the range 13–14 nm. *Quantum Electron.* **2001**, *31*, 683–688. [[CrossRef](#)]
20. Ivanova, E.P.; Ivanov, A.L. A superpowerful source of far-ultraviolet monochromatic radiation. *J. Exp. Theor. Phys.* **2005**, *100*, 844–856. [[CrossRef](#)]
21. Ivanova, E.P.; Grant, I. Oscillator strength anomalies in the neon isoelectronic sequence with applications to X-ray laser modeling. *J. Phys. B At. Mol. Opt. Phys.* **1998**, *31*, 2871–2883. [[CrossRef](#)]
22. Kramida, A.E.; Shirai, T. Energy levels and spectral lines of tungsten. W III through W LXXIV. *At. Data Nucl. Data Tables* **2009**, *95*, 305–474. [[CrossRef](#)]
23. Clementson, J.; Beiersdorfer, P.; Brown, G.V.; Gu, M.F. Spectroscopy of M-shell X-ray transitions in Zn-like through Co-like W. *Phys. Scr.* **2010**, *81*, 015301. [[CrossRef](#)]
24. Dong, C.-Z.; Fritzsche, S.; Xie, L.-Y. Energy levels and transition probabilities for possible X-ray laser lines of highly charged Ni-like ions. *J. Quant. Spectrosc. Rad. Transf.* **2003**, *76*, 447–465. [[CrossRef](#)]
25. Safronova, U.I.; Safronova, A.S.; Hamasha, S.M.; Beiersdorfer, P. Relativistic many-body calculations of multipole (E1, M1, E2, M2, E3, and M3) transitions wavelengths and rates between $3l^{-1}4l'$ excited and ground states in nickel-like ions. *At. Data Nucl. Data Tables* **2006**, *92*, 47–104. [[CrossRef](#)]
26. Stearns, D.G.; Rosen, R.S.; Vernon, S.P. Multilayer mirror technology for soft-X-ray projection lithography. *Appl. Opt.* **1993**, *32*, 6952–6960. [[CrossRef](#)] [[PubMed](#)]
27. Skulina, K.M.; Alford, C.S.; Bionta, R.M.; Makowiecki, D.M.; Gullikson, E.M.; Soufli, R.; Kortright, J.B.; Underwood, J.H. Molybdenum/beryllium multilayer mirrors for normal incidence in the extreme ultraviolet. *Appl. Opt.* **1995**, *34*, 3727–3730. [[CrossRef](#)] [[PubMed](#)]
28. Ivanova, E.P. X-ray laser near 13.5 and 11.3 nm in Xe²⁶⁺ driven by intense pump laser interacting with xenon cluster jet as a promising radiation source for nanolithography. *Laser Phys.* **2017**, *27*, 055802–055811. [[CrossRef](#)]
29. Makhotkin, I.A.; Zoethout, E.; Van de Kruijs, R.; Yakunin, S.N.; Louis, E.; Yakunin, A.M.; Banine, V.; Müllender, S.; Bijkerk, F. Short period La/B and LaN/B multilayer mirrors for 6.8 nm wavelengths. *Opt. Express* **2013**, *21*, 29894–29904. [[CrossRef](#)] [[PubMed](#)]
30. Dong, C.Z.; Fritzsche, S.; Gaigalas, G.; Jacob, T.; Sienkiewicz, J.E. Theoretical level structure and decay dynamics of Ni-like ions: search for laser lines in the soft X-ray domain. *Phys. Scr.* **2001**, *92*, 314–316.

